Article:
Zuo, J, Liu, Q, Meng, W et al. (2 more authors) (2023) Event-Triggered Adaptive Hybrid Torque-Position Control (ET-AHTPC) for Robot-Assisted Ankle Rehabilitation. IEEE Transactions on Industrial Electronics, 70 (5). pp. 4993-5003. ISSN 0278-0046

https://doi.org/10.1109/tie.2022.3183358

Event-Triggered Adaptive Hybrid Torque-Position Control (ET-AHTPC) for Robot-Assisted Ankle Rehabilitation

Jie Zuo, Quan Liu, *Member, IEEE,* Wei Meng*, Member, IEEE,* Qingsong Ai*, Member*, *IEEE,* and Sheng Quan Xie, *Senior Member, IEEE*

***Abstract*— Ankle rehabilitation for increasing number of strokes is highly demanded, and robot-assisted approach has shown great potential. Since the required movement and force assistances will concurrently change during rehabilitation sessions, the robotic assistances are supposed to be adjusted accordingly. In order to achieve both adaptive torque and synchronous position control for the robot in practice, a novel event-triggered adaptive hybrid torque-position control (ET-AHTPC) is proposed for a developed ankle rehabilitation robot driven by pneumatic muscles (PM). In the novel adaptive torque control scheme, the assistive torque adapted to the patient's recovery state is adjusted by a designed robot-assisted rehabilitation index mapping from the clinical assessment scale. The robotic assistance output is online corrected by patient's performance, based on a correcting index calculated by interaction torque and tracking errors. Then a model-based event-triggered optimal position controller is established and a critic neural network (NN) is introduced to reduce the control law update frequency for fast trajectory tracking. The stability of the overall system is proved by Lyapunov theorem. A series of experiments were conducted on the ankle rehabilitation robot to validate the controller's fast trajectory tracking and adaptive assistance capacity, which can online adjust the robot's assistive torque and allowable movement range for patients at different recovery stages.**

***Index Terms*— Ankle rehabilitation robot, event-triggered position control, adaptive torque control, adaptive assistance.**

I. Introduction

THE recent statistics reveal that the absolute number of strokes worldwide increased by 70.0% during the last two decades [1]. Most strokes have to suffer from the impaired ankle joint motor ability, which causes a serious negative impact on their daily life [2]. But the ankle motor ability of 90% strokes can be improved by appropriate rehabilitation training [2]. A medical study suggests that the position and force of the ankle for chronic strokes display concurrent changes, and thus the assistance needs to adapt to the joint's functional recovery and encourage the patient's voluntary participation [3].

To achieve this goal, interaction force/torque is one of the most common feedback adjustment signals applied in assisted-as-needed robotic rehabilitation system [4]. Asl *et al.* developed a force-field-based impedance controller for velocity tracking, to maximize the patient's active participation by limiting the movement in a velocity domain [5]. Baser *et al.* also proposed a force feedback impedance control approach a biomimetic compliant exoskeleton robot [6]. To further improve the stability and safety, Ballesteros *et al.* [7] and Ghannadi *et al.* [8] both proposed hybrid impedance-position control schemes, to achieve the best trade-off between tracking error and interaction force. But the methods did not consider the changes of required robotic assistance throughout rehabilitation. Mancisidor *et al.* proposed a complete set of training modes, including assistive, corrective and resistive, intended to adapt to the patient's rehabilitation needs in different sessions [9]. But the adjustment can only achieve the switch between three controllers (position, force, impedance). Naghavi *et al.* proposed a strength index-based force/position controller, and the control parameters could be adjusted according to the interaction force and tracking error [10]. Due to the multiple changing parameters of the robot assistance, a multi-modal control system is developed [11], which mainly aims to guarantee human safety. More attentions are expected on adjustment of the robotic assistance according to the patient's training performance and recovery states.

Due to the inner compliance, the pneumatic muscle (PM) displays better flexibility and is appropriately utilized as the rehabilitation robotic actuator. However, the inflation/ deflation working principle and highly-nonlinear and hysteresis characteristics of the PM make it difficult for PM-driven robots to quickly respond to the controller's frequent updates like rigid actuators [12]. Compared with time-driven control, event-triggered control improves response speed and synchronous performance of the multi-parameter control system, since the updates are only activated when the event-trigging condition is satisfied [13]. The event-triggered control has longer event-internal time and lower event-triggered frequency, thus remaining enough time to adjust the input of PM actuators. Further, the discrete characteristics of the event-triggered

Manuscript received February 1, 2022; revised May 5, 2022; accepted June 7, 2022. This work was supported in part by the National Natural Science Foundation of China under Grant 52075398 and Wuhan Application Frontier Project under Grant 2020020601012220. (Corresponding author: *Wei Meng*)

J. Zuo, Q. Liu, W. Meng, and Q. Ai are with the School of Information Engineering, Wuhan University of Technology, Wuhan, 430070, China (e-mails: {zuojie, quanliu, weimeng, qingsongai}@whut.edu.cn). Q. Ai is also with the School of Computer Science and Information Engineering, Hubei University, Wuhan, 430062 China.

S. Q. Xie is with the School of Electronic and Electrical Engineering, Leeds, LS2 9JT, UK. (e-mail: s.q.xie@leeds.ac.uk).

control scheme can greatly reduce the communication cost between the robot control system and the host computer database and applications. It is essential and beneficial to deeper studies of the practical robotic rehabilitation fields, e.g. with more different sensors applied in the human-robot interaction system, and the remote online application of the rehabilitation robot at home, etc.

However, most of the current event-triggered controllers are utilized for electric systems and multirobot systems [14-16], and only a few studies have been applied in robotic arms or exoskeletons [17-20]. Wu *et al.* proposed an event-triggered near-optimal tracking controller for robotic aircraft skin inspection, with a neural network (NN)-based observer for the disturbance compensation [20]. In [18], an event-triggered sliding mode controller (SMC) was developed to enhance the human-exoskeleton cooperation, and a genetic algorithm-back propagation NN is introduced to estimate the motion intention. Similarly, a sEMG-based event-triggered SMC scheme with deep differential NN was proposed for a lower limb exoskeleton [17]. An event-triggered motion-force controller is designed for the robotic ultrasonic examination, but it can only follow the fixed force [19]. Though the event-triggered control has been initially applied in the interaction-based robot trajectory tracking, the synchronous force/torque-position control with adjustable torque feedback has not been realized. Combining NNs with the controllers, the disturbance in the nonlinear system can be estimated and compensated during control. Deep NNs own good approximate performance with low learning rate for real-time control [21], while optimization-based algorithms raise the computational complexity and steady-state time [22]. Due to the simple structure and a prominent capacity for approximation, critic NN presents a faster convergence ability. The weight tuning laws of critic NN is simpler and the weights are updated according to the robot's historical state data only when the event-triggered condition is satisfied, thus it is more appropriate for the real-time robot control.

Thus, a new event-triggered adaptive hybrid torque-position control (ET-AHTPC) is proposed for a developed PM-driven ankle rehabilitation robot in this paper. The main contributions of this work include: 1) To synchronously adjust both robotic assistive torque and position output according to patient's performance in time, a novel hybrid torque-position control scheme is established with an adaptive torque control loop and an event-triggered position control loop. 2) To adapt to the motor ability and assistance requirement in different recovery stages, a robot-assisted rehabilitation index corresponding to the clinical assessment scale is designed and applied to adjust the assistive torque. 3) To enhance the real-time performance of the PM-driven robot in practice, a critic NN is introduced to update the event-triggered control parameters to reduce the update frequency, thus achieving fast trajectory tracking.

The rest of this paper is organized as follows. In Section II, an online adaptive torque control scheme is proposed. An event-triggered position controller with a critic NN is designed in Section III. Section IV presents experiments and analysis of the proposed controller conducted on the developed robot. The conclusion is summarized in Section V.

II. Adaptive Assistance Torque Control

Considering the human-robot interaction and tracking error, an online adaptive assistance torque control scheme is proposed. A robot-assisted rehabilitation index corresponding to the clinical assessment scale is designed and thus the torque control output can be adjusted according to the rehabilitation level.

A. Robot-Assisted Ankle Rehabilitation Platform

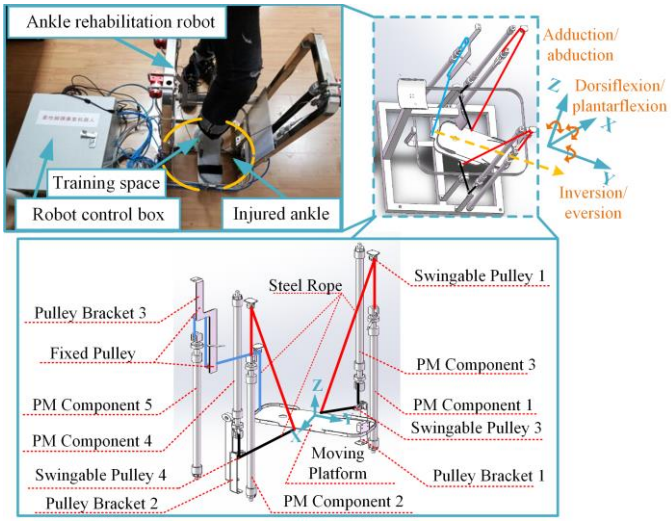

Fig. 1. Schematic diagram of the developed ankle rehabilitation robot.

During the actual rehabilitation sessions, the patient's motor ability and assistance needs are different. Brunnstrom scale is a common clinical assessment tool for the patient's motor ability, in which the stage III/IV/V are appropriate to facilitate ankle rehabilitation [23]. A 3-Degrees-of-Freedom (DOF) ankle rehabilitation robot driven by pneumatic muscles has been developed, as shown in Fig. 1. The moving platform of the robot mainly includes rotating joint 1/2/3 around X/Y/Z-axis and their support rods. To drive the moving platform, each PM is connected to the fixed point of the platform with the cable through the fixed/swinging pulley. PM 1 and PM 2 are responsible for the rotation around Y-axis, PM 3 and PM 4 achieve the rotation around Z-axis; PM 5, together with PM 1 and PM 2, enables rotation around X-axis. More details of the developed robot have been described in our previous work [24].The stage III/IV/V of Brunnstrom are mapped to Level-A/B/C in the robotic rehabilitation system, and define a robot-assisted rehabilitation index ω_{RI}. As presented in the previous research [24], the dynamic model of the robot is

$$M(q)\ddot{q} + C(q,\dot{q})\dot{q} + G(q) = \tau + \tau_{int} \qquad (1)$$

where $\dot{q}$ and $\ddot{q}$ respectively represent the first and the second derivatives of the robot's 3-DOF rotation angle vectors (X/Y/Z-axis) with respect to time. τ describes the robot's output torque, and τ_{int} is the human-robot interaction torque, both are 3×1 vectors. $M(q)$, $C(q,\dot{q})$ and $G(q)$ represent 3×3 inertia matrix and Coriolis force matrix and 3×1 gravity vector of the robot, respectively. More details about the modelling method and model parameters of the robot can be seen in Appendix. A.

Based on the robot platform, the total scheme of the proposed event-triggered adaptive hybrid torque-position controller (ET-AHTPC) is designed as Fig. 2.

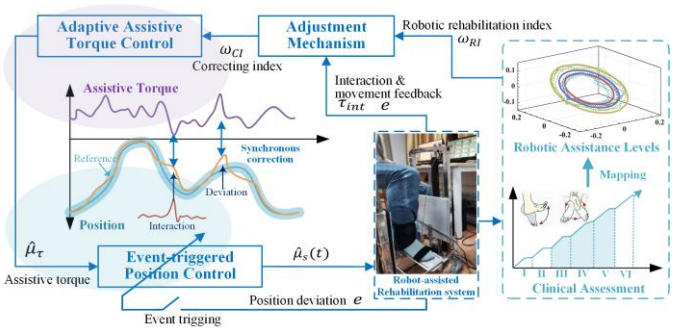

Fig. 2. The proposed ET-AHTPC scheme for ankle rehabilitation robot.

B. Feedback Weighting-Updated Torque Control

With the robotic assistance, the ankle should not only follow the desired trajectory, but also be encouraged to complete the training by the patient's voluntary participation. When the actual trajectory or the interaction torque deviates from the expected reference beyond the allowable boundary, the robot is triggered to synchronously adjust the position and torque output, to help the ankle return to the appropriate movement space.

To determine a suitable and safe movement space for the patient, the maximum movement range q_{max} of healthy subjects in the robot space is taken as reference, and the corresponding adjustment is made according to the patient's rehabilitation level ω_{RI}. Considering the patient's real-time training performance, the designed correcting index ω_{CI} is added, and its index was determined by the weight proportion result of balancing ω_{CI} and ω_{RI}. The parameter k_q and $\tanh(\cdot)$ are introduced to make the adjustment smoother. The allowable maximum movement region corresponding to the patient's state is defined as

$$q_{bound} = \tanh\left(k_q \omega_{CI}^3\right)\omega_{RI} q_{max} \tag{2}$$

where q_{max} is the robot's maximum movement angle vector and k_q is a constant. ω_{CI} is a correct index responding to both the tracking error e and interaction torque τ_{int}. If not otherwise specified in the following, the parameters related to robot dynamics, e.g. position or torque parameters, are 3×1 vectors.

$$\omega_{CI} = \frac{1}{\alpha_0 e^2 + \alpha_1 \tau_{int}^2 + 1} \tag{3}$$

where α_0 and α_1 are the corresponding weighting parameters of e and τ_{int}. The position error vector and velocity error vector are defined as $e = q - q_d$ and $\dot{e} = \dot{q} - \dot{q}_d$, where q_d, $\dot{q}_d$ represent the desired position and desired velocity of the robot.

In conventional controllers, the sliding surface is designed as $s = \dot{e} + ce$. To enhance the adaptivity of the torque controller, the new sliding surface is designed as

$$s = \dot{e} + c_r e \tag{4}$$

$$c_r = \begin{cases} 0, q \le q_{bound} \\ \omega_{RI}, \|q\| > q_{bound} \end{cases} \tag{5}$$

From (5), if the actual trajectory is inside the allowable region q_{bound}, s is designed to control the velocity only, allowing the patient's arbitrary movement but avoiding the abnormal motion speed. But if the actual trajectory is outside q_{bound}, the robot is driven back to the region according to the patient's motor ability as well as the position and interaction feedback.

Based on robot dynamic model in (1), the adaptive torque control law could be designed as

$$\mu_\tau = M(q)\ddot{q}_e + C(q,\dot{q})\dot{q}_e + G(q) - \alpha_\tau s + \varepsilon_{intc} \tag{6}$$

$$\varepsilon_{intc} = -\frac{s^T \tau_{int} + \sigma}{\|s^T \tau_{int}\| + \sigma}\tau_{int} \tag{7}$$

where $\dot{q}_e = \dot{q}_d + c_r e$. α_τ is a positive-definite matrix, and σ is a very small positive constant. From (7), if the interaction force τ_{int} is very large, i.e. $-\frac{s^T\tau_{int}+\sigma}{\|s^T\tau_{int}\|+\sigma} \approx -1$ and $\varepsilon_{intc} \approx -\tau_{int}$, the robot is driven by τ_{int} away from the desired trajectory, and the force adjustment vector ε_{intc} reinforces τ_{int}, and μ_τ is mainly adjusted by the interaction force. When τ_{int} is very small or even zero, i.e. ε_{intc} is small andμ_τ is mainly adjusted according to (5). If the tracking error is small, it means the patient is following the desired trajectory in the allowable region q_{bound} and should be encouraged; if not, the robotic assistance force would correct the patient's trajectory based on (6).

An observer $\hat{\dot{q}}_d$ is designed to estimate $\dot{q}_d$ and acceleration observer $\dot{\vartheta}$ is defined as follows, both are 3×1 vectors.

$$\hat{\dot{q}}_d = \vartheta + \beta_1 e_\Delta + c_r \hat{e} \tag{8}$$

$$\dot{\vartheta} = M^{-1}(q)\left(\varepsilon_{intc} - C(q,\dot{q})\vartheta + G(q) + \beta_y y + \beta_e e_\Delta\right) \tag{9}$$

where $y = \dot{q} - \vartheta$, $e_\Delta = q_d - \hat{q}_d$, $\hat{q}_d$ and $\hat{e}$ are the estimated values of q_d and e. β_1 is a positive constant, β_y and β_e are positive definite matrices. Thus the controller in (6) can be rewritten as follows, and the control diagram is shown in Fig. 3.

$$\hat{\mu}_\tau = M(q)\ddot{\hat{q}}_e + C(q,\dot{q})\dot{\hat{q}}_e + G(q) - \alpha_\tau \hat{s} + \varepsilon_{intc} \tag{10}$$

where $\hat{s} = \dot{q} - \dot{\hat{q}}_d + c_r\hat{e}$, $\dot{\hat{q}}_e = \dot{\hat{q}}_d + c_r\hat{e}$.

C. Stability Analysis

To analyze the stability of the torque control loop, the Lyapunov function is developed as

$$V = \frac{1}{2}\hat{s}^T M(q)\hat{s} + \frac{1}{2}y^T M(q) y \tag{11}$$

Differentiating (11) with respect to time, yields

$$\dot{V} = \hat{s}^T M(q)\dot{\hat{s}} + y^T M(q)\dot{y} \tag{12}$$

Combining (1), (9) and (10), (12) can be rewritten as

$$\dot{V} = \hat{s}^T(\varepsilon_{intc} + \tau_{int}) - y^T\beta_y y - \Lambda_1\Lambda_\beta\Lambda_1^T \tag{13}$$

where $\Lambda_1 = [\hat{s}^T \quad e_\Delta^T]$, $\Lambda_\beta = \begin{bmatrix} \alpha_\tau & \frac{1}{2}\beta_e \\ \frac{1}{2}\beta_e & \beta_1\beta_e \end{bmatrix}$.

Without human interaction, i.e. $\varepsilon_{intc} = 0$, (13) is rewritten as

$$y^T\beta_y y + \Lambda_1\Lambda_\beta\Lambda_1^T + \dot{V} = \hat{s}^T\tau_{int} \tag{14}$$

If Λ_β is positive definite, (15) is guaranteed, which has been detailed proved in [11]. And $\hat{s}^T(\varepsilon_{intc} + \tau_{int})$ in (13) is written as (16). The detailed derivation is shown in Appendix. B.

$$y^T\beta_y y + \Lambda_1\Lambda_\beta\Lambda_1^T \ge 0 \tag{15}$$

$$\hat{s}^T(\varepsilon_{intc} + \tau_{int}) = \hat{s}^T \Lambda_\sigma \tau_{int} \tag{16}$$

where $\Lambda_\sigma = 1 - \frac{s^T \tau_{int} + \sigma}{\|s^T \tau_{int}\| + \sigma}$. When $\hat{s}^T \tau_{int} \geq 0$, $\Lambda_\sigma = 0$; when $\hat{s}^T \tau_{int} < 0$, $\Lambda_\sigma \geq 0$. Thus

$$\hat{s}^T(\varepsilon_{intc} + \tau_{int}) \leq 0 \tag{17}$$

Substituting (15) and (17) into (13), we have $\dot{V} \leq 0$. Thus it can be concluded that the torque control loop is stable.

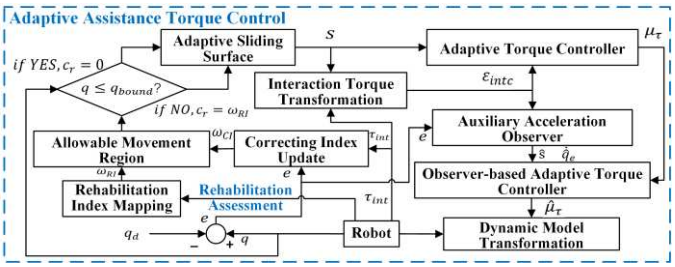

Fig. 3. The proposed adaptive torque control scheme.

III. Event-Triggered Position Control

A novel event-triggered optimal position control scheme is proposed based on the robot dynamic model. A critic NN is applied to update the parameters of the control law under the event-trigging condition, to reduce the update frequency of the control law. With the adaptive torque input, the controller could achieve efficient synchronously torque-position control for the robot-assisted rehabilitation in practice.

A. Event-Triggered Optimal Position Control

Based on the dynamic model in (1) and inverse kinematics of the designed robot, the control object is defined as

$$\begin{cases} \dot{x}_1 = x_2 \\ \dot{x}_2 = f(x) + g(x)\mu_s + \beta_\delta \delta_e \end{cases} \tag{18}$$

where μ_s is the control signal vector, x is the control state vector of the robot, and $\beta_\delta \delta_e$ represents the bounded disturbance vector. δ_e (3×1) denotes the system comprehensive disturbances not involved in the robot dynamic model, including disturbances caused by the PM's nonlinearity, human-robot interaction, etc. For the event-triggered controller μ_s, a monotonically increasing sequence of event triggering instants $\{z_j\}_j^\infty$ is set up. z_j represents the j th consecutive triggering instant, i.e. the moment of jth event occurred, and $z_j < z_{j+1}$. The state vector at the triggering component is defined as $\hat{x}_j = x(z_j)$ for $t \in [z_j, z_{j+1})$. Then based on zero-order hold (ZOH), the trigger error vector $e_j(t)$ is expressed as the function between the sampled states and the current value, and the obtained control sequence can be converted into continuous input signals by ZOH [25].

$$e_j(t) = \hat{x}_j(t) - x(t), \forall\, t \in [z_j, z_{j+1}) \tag{19}$$

Thus the event-triggered controller in (18) is rewritten as

$$\dot{x} = f(x(t)) + g(x(t))\mu_s\left(x(t) + e_j(t)\right) + \beta_\delta \delta_e, \quad \forall\, t \in [z_j, z_{j+1}) \tag{20}$$

Based on Hamiltonian dynamics, the energy trajectory moves within a hypersurface of probability density determined by dynamics of the control system, i.e. the system energy can be expressed as the control function in the process. Define the performance index Φ_{PI} for the controller as (21). The hyperbolic tangent function $\tanh(\cdot)$ is employed for smoother, and $\tanh^{-T}(\cdot)$ is the inverse transpose of $\tanh(\cdot)$.

$$\Phi_{PI}(\mu_s) = 2\varepsilon \int_0^{\mu_s} \tanh^{-T}\left(\frac{\mu_s}{\varepsilon}\right) K d\mu_s \tag{21}$$

where $\varepsilon \geq \|\mu_s\|$, and $K \in \mathbb{R}^{3\times 1}$. From the integral solution of (21), it is rewritten as

$$\Phi_{PI}(\mu_s) = 2\varepsilon \mu_s{}^T K \tanh^{-1}\left(\frac{\mu_s}{\varepsilon}\right) + \varepsilon^2 \widetilde{K} \ln\left(1 - \left(\frac{\mu_s}{\varepsilon}\right)^2\right) \tag{22}$$

where $\widetilde{K} \in \mathbb{R}^{1\times m}$. In time-triggered controllers, it is satisfied as

$$\int_t^\infty \left(x^T R x + \Phi_{PI}(\mu_s)\right) d\tau \leq \varrho^2 \int_t^\infty \delta_e{}^T \delta_e d\tau \tag{23}$$

where $\varrho > 0$, and R is a positive matrix.

Then the performance function and the cost function of the time-triggered controller is defined as

$$\mathcal{J}(\mu_s, \delta_e) = \int_0^\infty \left(x^T R x + \Phi_{PI}(\mu_s) - \varepsilon^2 \delta_e{}^T \delta_e\right) d\tau \tag{24}$$

$$\mathcal{Q}(x) = \int_t^\infty \left(x^T R x + \Phi_{PI}(\mu_s) - \varepsilon^2 \delta_e{}^T \delta_e\right) d\tau \tag{25}$$

Then the Hamiltonian function is

$$\mathcal{H}(\mathcal{Q}, \mu_s, \delta_e) \triangleq x^T R x + \Phi_{PI}(\mu_s) - \varepsilon^2 \delta_e{}^T \delta_e + \tilde{\mathcal{Q}}^T \dot{x} = 0 \tag{26}$$

where $\tilde{\mathcal{Q}} = \frac{\partial \mathcal{Q}(x)}{\partial x}$.

For the designed event-triggered controller, the performance function (24) can be expressed as

$$\mathcal{J}(\mu_s(\hat{x}_j), \delta_e) = \sum_{\cup_j [z_j, z_{j+1}) = [0,\infty)} \int_{z_j}^{z_{j+1}} \left(x^T R x + \Phi_{PI}(\mu_s) - \varepsilon^2 \delta_e{}^T \delta_e\right) d\tau \tag{27}$$

The control law $\mu_s(\hat{x}_j)$ is updated when the event is triggered at the moment of z_j. For the control object in a nonlinear system as (18), its solution is usually based on Hamilton–Jacobi–Isaacs (HJI) equation. To optimize the control law and event-triggered intervals at the same time, the event-triggered control law needs to satisfy the Nash equilibrium solution corresponding to the HJI equation [26]. The control law and disturbance item are rewritten as

$$\mu_s(\hat{x}_j) = -\varepsilon \tanh\left(\frac{K^{-1} g^T(\hat{x}_j) \tilde{\mathcal{Q}}(\hat{x}_j)}{2\varepsilon}\right), \forall\, t \in [z_j, z_{j+1}) \tag{28}$$

$$\delta_e(\hat{x}_j) = \frac{\beta_\delta{}^T \tilde{\mathcal{Q}}(\hat{x}_j)}{2\varepsilon^2} \tag{29}$$

The control law μ_s is Lipschitz continuous with respect to the event-triggering error according to [13], which is a stricter smoothness condition than the usual continuous.

$$\left\|\mu_s(x(t)) - \mu_s(\hat{x}_j)\right\| \leq \mathcal{L}_u \|e_j(t)\| \tag{30}$$

where $\mathcal{L}_u$ is a positive parameter.

Based on (26), (28) and (29), the triggering condition is

$$\|e_j(t)\|^2 \leq \frac{(1-\eta)\lambda_{\min}[R]\|x\|^2}{\varepsilon^2 \mathcal{L}_u^2 \|K\|} + \frac{\Phi_{PI}\left(\mu_s(\hat{x}_j)\right)}{\varepsilon^2 \mathcal{L}_u^2 \|K\|} - \frac{\|\varrho\|^2 \|\delta_e\|^2}{\varepsilon^2 \mathcal{L}_u^2 \|K\|} \triangleq e_T \tag{31}$$

where η is a parameter of the sampling frequency. e_T is the triggering threshold. If the condition (30) is satisfied, the event is triggered and the control law will be updated.

For the continuous-time system, the minimum trigger interval may be zero if the event trigger control method is adopted. This would cause the event to be fired infinite times, thus making the controller update an infinite number of times, which is called Zeno behavior [27]. To avoid Zeno behavior, the minimum sample time z_{min} should satisfy the condition:

$$z_{min} \geq \frac{1}{\kappa_{z1}} \ln\left(1 + \min_{j \in N} \frac{\left\|e_j(t)\right\|^2}{\left\|\hat{x}_j\right\|^2 + \kappa_{z2}}\right) > 0 \tag{32}$$

where κ_{z1} and κ_{z2} are positive constants. Since the proof is similar to that in [28], it is omitted here.

B. Critic NN-Updated Event-Triggered Control

As for optimization of the nonlinear system, it is challenging to minimize the cost function in the worst-case disturbance, i.e. to find the solution for HJI equations of the PM-driven robot, which is a nonlinear system with partially unknown disturbance. Critic NN possesses the capability of real-time learning control and faster convergence than other deep NNs. Combined with the Weierstrass approximation, critic NN can adjust the weights according to the historical data of the robot's certain performance, with fewer data requirement and shorter initial learning phase than supervisory learning. The weight tuning laws of the critic NN is simpler and updated only when the event-triggered condition is satisfied, which is appropriate for the PM-driven robotic rehabilitation system.

Thus critic NN is employed to approximate the optimal solution of $Q(x)$, μ_s and δ_e. Based on Weierstrass high-order approximation, the approximation of $Q(x)$ and $\tilde{Q}(x)$ are

$$Q(x) = \omega_c^T \sigma_c(x) + \epsilon_c \tag{33}$$

$$\tilde{Q}(x) = \nabla \sigma_c^T(x) \omega_c + \nabla \epsilon_c \tag{34}$$

where ω_c denotes the ideal weight vector, $\sigma_c(x)$ is the activation function, and ϵ_c represents the approximated error of the critic NN. And assume that $\|\omega_c\| \leq \omega_{cmax}$, $\|\sigma_c\| \leq \sigma_{cmax}$, and $\|\epsilon_c\| \leq \epsilon_{cmax}$. Then the approximated cost function is

$$\hat{Q}(x) = \hat{\omega}_c^T \sigma_c(x) \tag{35}$$

where $\hat{\omega}_c$ is the estimation vector of ω_c, and the estimation error vector is defined as $\tilde{\omega}_c = \omega_c - \hat{\omega}_c$.

Based on (18) and (32), HJI function in (26) is rewritten as

$$\begin{aligned} \mathcal{H}(x, \omega_c) &= x^T R x + \Phi_{PI}\left(\mu_s(\hat{x}_j)\right) - \varepsilon^2 {\delta_e}^T \delta_e \\ &+ \omega_c^T \sigma_c(x)(f + g\mu_s(\hat{x}_j) + \beta_\delta \delta_e) \triangleq \Psi_h \end{aligned} \tag{36}$$

Then the estimated function of (20) is

$$\begin{aligned} \hat{\mathcal{H}}(x, \omega_c) &= x^T R x + \Phi_{PI}\left(\hat{\mu}_s(\hat{x}_j)\right) - \varepsilon^2 {\hat{\delta}_e}^T \hat{\delta}_e \\ &+ \hat{\omega}_c^T \nabla \sigma_c(x)\left(f + g\hat{\mu}_s(\hat{x}_j) + \beta_\delta \hat{\delta}_e\right) \triangleq \hat{\Psi}_h \end{aligned} \tag{37}$$

Define $\mathcal{u} = x^T R x + \Phi_{PI}\left(\hat{\mu}_s(\hat{x}_j)\right) - \varepsilon^2 {\hat{\delta}_e}^T \hat{\delta}_e$, $\mathcal{v} = \nabla \sigma_c(x)\left(f + g\hat{\mu}_s(\hat{x}_j) + \beta_\delta \hat{\delta}_e\right)$, thus $\hat{\Psi}_h = \mathcal{u} + \hat{\omega}_c^T \mathcal{v}$. The stored sample data at $t_r \in [z_j, z_{j+1}]$ is $\Psi_e(t_r) = \mathcal{u}_r + \hat{\omega}_c^T \mathcal{v}_r$, where $\mathcal{u}_r = x(t_r)^T R x(t_r) + \Phi_{PI}\left(\hat{\mu}_s(\hat{x}_j)\right) - \varepsilon^2 \hat{\delta}_e(t_r)^T \hat{\delta}_e(t_r)$ and $\mathcal{v}_r = \nabla \sigma_c(x(t_r))\left(f + g\hat{\mu}_s(\hat{x}_j) + \beta_\delta(t_r)\hat{\delta}_e(t_r)\right)$. To guarantee the persistence of the activation condition, the adaptive weight law of the critic NN $\hat{\omega}_c$ is designed as (38) to obtain the minimum value of residual error.

$$\dot{\hat{\omega}}_c = \frac{-\varphi \mathcal{v}(\mathcal{u} + \hat{\omega}_c^T \mathcal{v})}{(\mathcal{v}^T \mathcal{v} + 1)^2} + \sum_{t_r=1}^{N} \frac{-\varphi \mathcal{v}_r(\mathcal{u}_r + \hat{\omega}_c^T \mathcal{v}_r)}{({\mathcal{v}_r}^T \mathcal{v}_r + 1)^2} \tag{38}$$

where φ is the learning rate of critic NN and N is the number of stored samples. Within the adaptive event-triggered control, critic NN can quickly approximate the cost function and shorten the convergence time, due to its learning capability from both cost function and the stored sample data as shown in (38). Then with the quickly convergent weight vector, a novel event-triggered optimal control law is developed.

Thus the estimated event-triggered control law in (28) and the disturbance item in (29) can be established as (39). The control diagram is shown in Fig. 4.

$$\hat{\mu}_s(t) = -\varepsilon \tanh\left(\frac{K^{-1} g^T(\hat{x}_j) \nabla \sigma_c^T(\hat{x}_j) \hat{\omega}_c}{2\varepsilon}\right), \forall\, t \in [z_j, z_{j+1}) \tag{39}$$

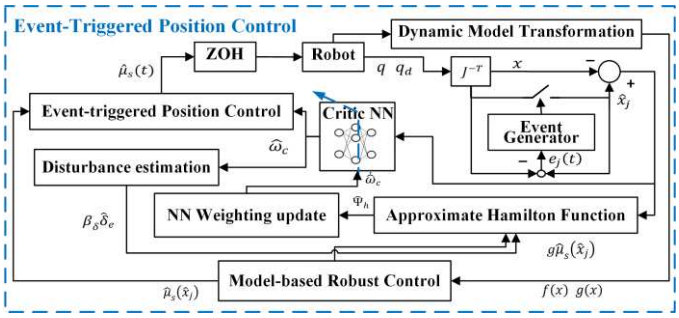

Fig. 4. The proposed event-triggered position control scheme.

C. Stability Analysis

For the event-triggered position control loop, the stability analysis consists of two cases: the state of not triggered and the event-triggered state. The Lyapunov function V composes the function of continuous state V_x, jump state $V_{\hat{x}_j}$ and critic NN V_c.

$$V = V_x + V_{\hat{x}_j} + V_c \tag{40}$$

1) *When an event is not triggered.* Since in the continuous inter-event interval $\forall\, t \in [z_j, z_{j+1})$, the event is not triggered, i.e. the triggering item does not work. Thus it is written as

$$V = V_x + V_c = \tilde{Q} + \frac{1}{2\varphi} tr\{\tilde{\omega}_c^T \tilde{\omega}_c\} \tag{41}$$

According to (26) and (27), define V_x as the Lyapunov function for the continuous event-triggered controller, thus

$$\dot{V}_x = \tilde{Q}^T f + \tilde{Q}^T g \hat{\mu}_s(\hat{x}_j) + \tilde{Q}^T \beta_\delta \hat{\delta}_e \tag{42}$$

Based on (26), (29) and (39), the event-triggered HJI at the moment $t = z_j$ is

$$x^T R x + \tilde{Q}^T f + \Phi_{PI}\left(\hat{\mu}_s(\hat{x}_j)\right) + \tilde{Q}^T g \hat{\mu}_s(\hat{x}_j) + \frac{\tilde{Q}^T \beta_\delta \beta_\delta^T \tilde{Q}}{4\varrho^2} = 0 \tag{43}$$

Then combined with (29) and (43), (42) can be derived as

$$\begin{aligned} \dot{V}_x = &\int_{\hat{\mu}_s(x)}^{\hat{\mu}_s(\hat{x}_j)} 2\varepsilon K \hat{\mu}_s^T K d\tau + 2\varrho^2 \delta_e^T \hat{\delta}_e - \varepsilon \tilde{Q}^T g \tanh(\hat{\mu}_s) \\ &- \varepsilon^2 \tilde{K} \ln\left(1 - \tanh^2 \hat{\mu}_s\right) - x^T R x - \varrho^2 \delta_e^T \delta_e \end{aligned} \tag{44}$$

Due to the Young's inequality, (44) is rewritten as

$$\dot{V}_x \leq 2\varepsilon^2 \left(\mathcal{L}_u^2 \|K\| \left\|e_j(t)\right\| - \left\|\mu_s(x) - \hat{\mu}_s(x)\right\|^2\right) \tag{45}$$

When the event-trigging condition in (31) is satisfied, it can be obtained from (45) that

$$\dot{V}_x \le 2\varepsilon^2 \left\| \mu_s(x) - \hat{\mu}_s(x) \right\|^2 < 0 \tag{46}$$

Thus the system of the continuous control is proved to be asymptotically stable.

From the above analysis about the critic NN in (38), the persistence of excitation condition is guaranteed, thus $\dot{V}_c$ is satisfied the following condition [29].

$$\dot{V}_c \le -\eta_c \lambda_{\min}\left[\frac{\upsilon}{\upsilon^T\upsilon+1}\right]\|\tilde{\omega}_c\|^2 + \eta_c\|\tilde{\omega}_c\|\Psi_{hm} \tag{47}$$

where η_c and Ψ_{hm} are positive constants, and $\eta_c > 1$. According to Young's inequality, (47) is derived as

$$\dot{V}_c \le (1-\eta_c)\lambda_{\min}\left[\frac{\upsilon}{\upsilon^T\upsilon+1}\right]\|\tilde{\omega}_c\|^2 + \frac{\eta_c^2\Psi_{hm}^2}{4} \tag{48}$$

Thus the second item of (48) is bounded, and the system is proved to be asymptotically stable. $\|\tilde{\omega}_c\|$ needs to satisfy:

$$\|\tilde{\omega}_c\| \ge \sqrt{\eta_c^2\Psi_{hm}^2 / \left(4(\eta_c-1)\lambda_{\min}\left[\frac{\upsilon}{\upsilon^T\upsilon+1}\right]\right)} \tag{49}$$

2) *When an event is triggered.* The difference between the Lyapunov function of the event-triggered condition from that of (41) is at the triggering moment $\forall\, t = z_j$, thus

$$\Delta V = \Delta V_x(x) + \Delta V_{\hat{x}_j} + \Delta V_c \tag{50}$$

According to (46) and (48), the first and third items are both asymptotically stable, i.e. $\Delta V_x(x) \le 0$ and $\Delta V_c(x) \le 0$. Then we have

$$\Delta V_{\hat{x}_j} = \tilde{\mathcal{Q}}(\hat{x}_{j+1}) - \tilde{\mathcal{Q}}(\hat{x}_j) \le -\kappa\left\|e_j(t)\right\| \tag{51}$$

where κ is a class- κ function.

Substituting (51) into (50), yields

$$\Delta V \le -\kappa\left\|e_j(t)\right\| \tag{52}$$

Thus the controller at the state of event-trigging is also proved to be stable.

IV. Experiments and Results Discussion

To validate the event-triggered control performance and the adaptive synchronous torque-position control capacity of the proposed ET-AHTPC, two groups of experiments were conducted on the developed ankle rehabilitation robot. Due to the rehabilitation requirement of low-frequency reciprocating movements, the robot's desired trajectory was set as $q_{xd} = 0.2\cos(2\pi f t)$ (rad), $q_{yd} = 0.2\sin(2\pi f t)$ (rad), and $q_{zd} = 0.1\sin(2\pi f t)$ (rad), $f = 0.05Hz$. Healthy subjects were asked to put their feet on the robot platform and follow the robot's movement. To initially validate the control performance of the ET-AHTPC for patients at different rehabilitation stages, the healthy subjects were instructed to wear medical bandages of different widths and tightness on the ankle to weaken the joint's motor ability. The trials were approved by Human Participants Ethics Committees from Wuhan University of Technology, and written informed consent was obtained from each participant. Since the robot-assisted rehabilitation index $\omega_{RI} \in (0,1)$ mapping from the Brunnstrom, the value was set as 0.8, 0.5, 0.2 corresponding to Level-A/B/C in the experiments. As presented in Fig. 5, larger movement space is allowable from Level-A to Level-C, which satisfies the ankle rehabilitation needs. In the experiments, the initial critic NN weights are all set as 0.2, and the learning rate φ=18. Other control parameters are selected as: η= 0.5, $\mathcal{L}_u$=4, ϱ=1 R=diag [10, 10], K=0.02, κ_{z1}=2, κ_{z2}=0.01, α_τ =1, σ =10^{-5}, β_1 =100 , β_y =1, β_e =50. The initial control parameters including the weights of critic NN are selected from a reasonable range in simulation experiments, to enable the proposed controller to achieve a high tracking accuracy. The weights of critic NN are randomly generated within [-1.5 1.5] for 40 trials with 200-time steps, to obtain a set of weights that are all convergent quickly. After the training, the selected weights are kept unchanged for the following experiments. Then selected parameters are adjusted in repeated experiments on the real robotic platform, and the termination condition $\varepsilon = 10^{-5}$ to achieve approximate optimal control.

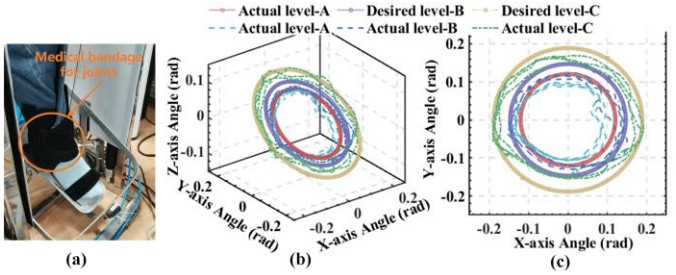

Fig. 5. The designed robot-assisted ankle rehabilitation levels. (a) The developed ankle rehabilitation robot platform; (b) and (c) are corresponding to the 3D/2D movement space of Level-A/B/C.

A. Event-Triggered Position Control

By utilizing the proposed event-triggered controller and setting the parameters as described above, the critic NN weights converge to ω_c =[0.7693, -1.2165, 1.0384, -0.4528, 0.5761] after 0.3 s for iterating 20 times, as shown in Fig. 6 (a).

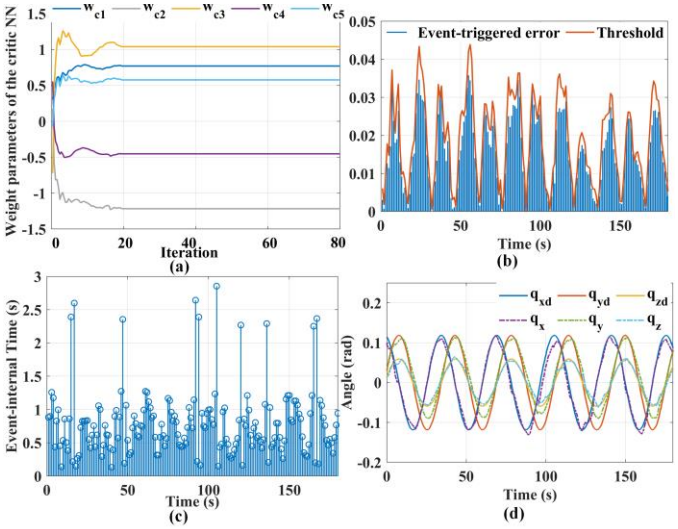

Fig. 6. The performance of the proposed event-triggered position control scheme for the robot-assisted ankle rehabilitation. (a) Convergence of the critic NN weights; (b) Evolution of the event-triggered error and threshold; (c) Event interval time of control during the learning process; (d) Trajectory tracking performance under the event-triggered control.

From Fig. 6 (b) and (c), the updates only occur when the event-triggered condition is satisfied, thus the updating frequency of the control law is much lower than time-driven

controllers [30]. Fig. 6 (d) proves the proposed controller's accurate tracking performance. As seen from Table I, event-triggered controllers (ETC) [18, 19] have a faster response than time-driven controllers (TDC) [31, 32], and the former can also achieve stable and accurate tracking. However, the few existing ETC research for robots are mostly simulation. To adapt to the working characteristics of the PM-driven robot, the ET-AHTPC has longer event-internal time and lower event-triggered frequency compared with that of [31, 32], thus remaining enough time to adjust the input of PM actuators. In comparison with the simulation results in [31, 32], the tracking error of the proposed controller is also acceptable.

TABLE I
PERFORMANCE COMPARISON OF ADVANCED TIME-DRIVEN CONTROLLERS AND EVENT-TRIGGERED CONTROLLERS

Reference	Type	Event-triggered count (100s)	Response Time (s)	Tracking error		
				ME (%)	AE (%)	RMSE (%)
[31]	TDC	*	2.0	12.50	*	*
[32]	TDC	*	7.0	*	4.25	*
[19]	ETC	170	0.4	*	*	1.25
[18]	ETC	204	0.3	*	*	2.41
ET-AHTPC	ETC	83	0.3	6.74	2.83	1.47

* = The unknown value, ME = Maximum error, AE = Average error, RMSE = Root mean square error.

To demonstrate the effect of critic NN on the event-triggered control strategy, a comparison experiment of the controllers with or without critic NN was conducted, and results are shown in Fig. 7. It can be seen that the position and torque tracking of the controller without critic NN presents a delay compared with the one with critic NN, since critic NN can enhance the convergence speed of the event-triggered controller, reducing the tracking errors as well as the number of events triggered. Due to the discrete characteristics of the event-triggered controller, its position and torque tracking curves appear to be toothed. While the critic NN's fast update and convergence capability make the robot's control output more stable and smoother, which is essential for robotic rehabilitation application.

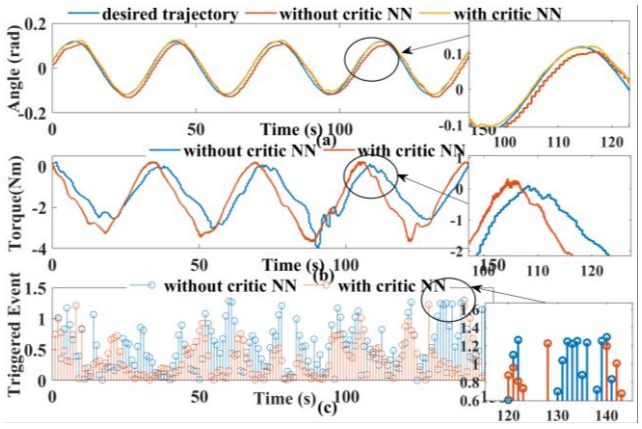

Fig. 7. The comparison of the event-triggered controller with/without critic NN. (a) The trajectory tracking performance; (b) The interaction torque and assistive torque output by the robot; (c) The triggered events during the control process.

For further validation of the proposed event-triggered controller's fast-response and its synchronous torque-position control capacity, abrupt changes of the position and human-robot interaction were applied in the experiments, and results are shown in Fig. 8 and Fig. 9. When the subject exerts a sudden position deviation from the desired trajectory, the error is large enough to activate the event-triggered condition and the control law is updated to drive the robot to quickly follow the desired trajectory, as shown in Fig. 8. During the control process, the robotic assistive torque also displays a fast response with small adjustments when the abrupt deviation occurs. Similarly, when the subject suddenly changes the interaction force applied to the robot (Fig. 9), the assistive torque quickly corrects in the opposite direction of the interaction to drive the movement back into the allowable region. The abrupt position error also triggered the event and the trajectory is adjusted at the same time. These two cases validate that the proposed ET-AHTPC guarantees the stability and adaptivity of the synchronous torque-position control system, which are significant for robot-assisted rehabilitation in practice.

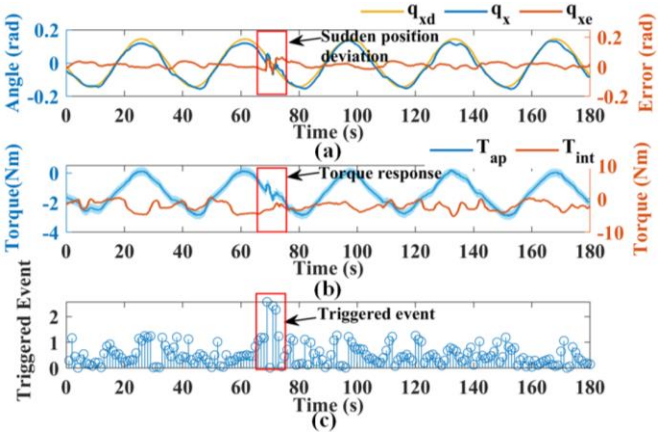

Fig. 8. The performance of the proposed event-triggered controller under the sudden position deviation. (a) The trajectory tracking performance; (b) The interaction torque and assistive torque output by the robot; (c) The triggered events during the process.

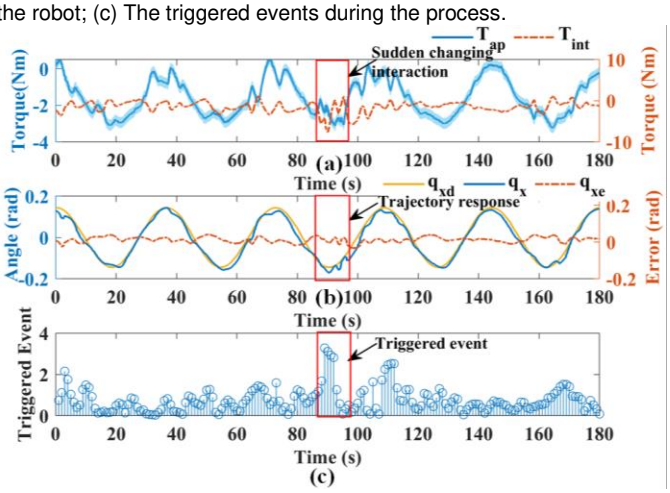

Fig. 9. The performance of the proposed event-triggered control scheme under the sudden changing human-robot interaction. Take the experimental data around X-axis as an example. (a) The assistive torque output towards the changing interaction torque; (b) The trajectory tracking performance; (c) The triggered events during the process.

B. Adaptive Robotic Assistance

In this section, the adaptive synchronous torque-position assistance capacity of the proposed ET-AHTPC according to the patient's real-time performance and rehabilitation state will be proved by the experiments. Firstly, two cases of adjusting ω_{RI} were carried out, as shown in Fig. 10. When the value of ω_{RI} is changed from 0.5 to 0.2, the assistance level is switched from Level-B to Level-C, i.e. it steps into a better rehabilitation stage, thus the robot would provide larger motion space and less assistance, as presented in Fig. 10 (a) and (b). The assistive torque is reduced to encourage the subject's voluntary participation. Then when the level is switched from Level-C to Level-B, the allowable movement space is smaller, and larger assistive torque is output to drive the subject to follow the desired trajectory (Fig. 10 (c) and (d)). As seen from Table II, the ET-AHTPC can achieve trajectory/ torque fast-tracking at the same time, and the errors are always within an acceptable range. Thus ET-AHTPC's synchronous torque-position adjustment for different rehabilitation sessions is proved.

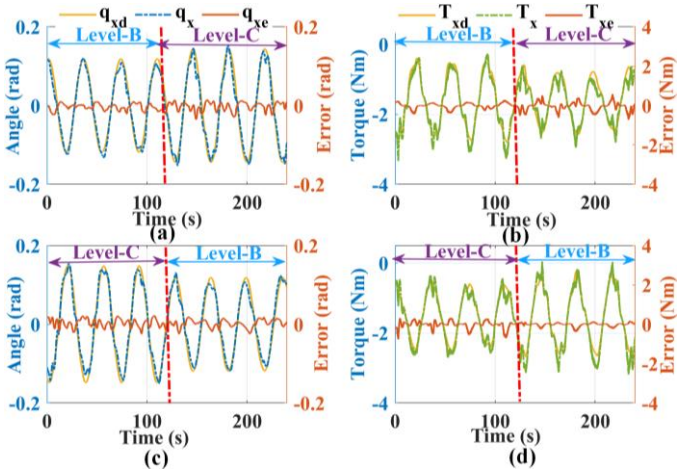

Fig. 10. The adaptive assistance capacity of the proposed ET-AHTPC when switching the rehabilitation index ω_{RI}. Take the experimental data around X-axis as an example. (a) and (b) present the trajectory and assistance tracking performance of the robot from Level-B to Level-C; (c) and (d) present the trajectory and assistance tracking performance of the robot from Level-C to Level-B.

TABLE II
CONTROL PERFORMANCE UNDER THE ET-AHTPC UNDER LEVEL SWITCHING

Axis	Position RMSE (*10^{-2} rad)				Torque RMSE (*10^{-2} Nm)			
	Case I: B to C		Case II: C to B		Case I: B to C		Case II: C to B	
	B	C	C	B	B	C	C	B
X	1.46	1.93	2.01	1.60	4.34	6.05	5.82	3.97
Y	1.23	1.78	1.82	1.31	3.67	5.19	5.02	3.21
Z	0.75	0.86	0.91	0.83	2.59	3.81	3.69	2.46

For further validation of the ET-AHTPC's adaptivity and robustness towards different users, four healthy subjects were recruited to participate in the following experiments, and their basic information is presented in Table III. From Fig.11, the robotic assistive torques compared to the standard are within the range of 20.09%-58.85% for different rehabilitation levels. The robotic assistance is generally reduced by nearly 40% from Level-A to Level-C, and the larger movement freedom could maximize the patient's voluntary participation based on his/her rehabilitation state. As shown in Table IV, though the allowable deviation range of the position and torque are both increased from Level-A to Level C, the errors of all subjects are limited to an acceptable range to guarantee the movement safety. The maximum position and torque tracking RSME of four subjects are 0.0210 rad and 0.0663 Nm respectively, which also verifies the robustness of the proposed ET-AHTPC towards different subjects.

To confirm the ET-AHTPC's synchronous torque-position adjustment capacity, a comparison is conducted with relevant studies [33-35]. As seen from Table V, the position tracking performance in [33] is better than the ET-AHTPC, but the former only achieved single control of the position or torque in a training mode. Compared with [33-35], ET-AHTPC displays more stable and accurate performance for synchronous position-torque control even at different training levels. From Fig. 12, the distribution of the assistive torque changes smoothly with the trajectory in the whole motion space even across levels. It is proved that the proposed controller can realize smooth and synchronous adjustment of the robot's position and torque, so as to provide more naturally adaptable assistance for patients.

TABLE III
INFORMATION OF THE PARTICIPATED HEALTHY SUBJECTS

Subjects	Gender	Age	Height (cm)	Weight (kg)
Subject 1 (S1)	Female	28	168	61
Subject 2 (S2)	Male	24	178	73
Subject 3 (S3)	Male	25	174	65
Subject 4 (S4)	Female	23	162	52

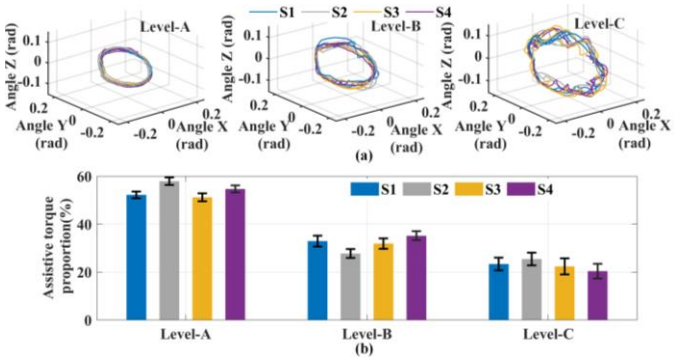

Fig. 11. The adjustable position/torque control performance of the proposed ET-AHTPC for the robotic ankle rehabilitation with four subjects at different levels. (a) includes the trajectory tracking results of Level-A/B/C; (b) presents the proportion of robotic assistive torque relative to the standard torque of human ankle in different levels.

TABLE IV
CONTROL PERFORMANCE UNDER THE PROPOSED ET-AHTPC WITH DIFFERENT SUBJECTS

Subjects	Position RSME (*10^{-2} rad)			Torque RSME (*10^{-2} Nm)		
	Level-A	Level-B	Level-C	Level-A	Level-B	Level-C
S1	0.93	1.53	1.82	2.88	4.58	5.37
S2	1.26	1.39	1.98	3.09	3.70	5.28
S3	0.87	1.64	2.10	3.37	4.34	6.63
S4	1.18	2.03	2.04	2.93	3.77	6.11
Mean	1.06	1.65	1.98	3.07	4.10	4.71

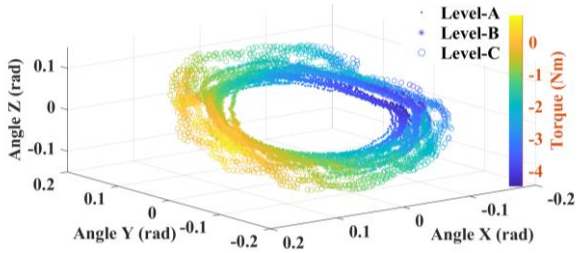

Fig. 12. The synchronous performance of position/torque adjustment of the ET-AHTPC in the whole robot-assisted rehabilitation space.

TABLE V
PERFORMANCE COMPARISON OF ADVANCED FORCE/TORQUE-POSITION CONTROLLERS FOR REHABILITATION ROBOTS

Reference	Rehabilitation Joint	Modes	Position RMSE	Torque RMSE
[33]	Wrist and forearm	Passive	1.59%	*
		Active	3.02%	*
		Isometric	*	21.26%
		Isotonic	*	30.71%
[34]	Wrist	Passive	2.80%	7.16%
		Active	*	20.83%
		Resistive	*	*
[35]	Hip and knee	Passive	5.57%	6.70%
		Active	12.57%	21.66%
ET-AHTPC	Ankle	Level-A	2.65%	6.14%
		Level-B	4.12%	10.25%
		Level-C	5.05%	15.70%

V. CONCLUSION

In this paper, a novel ET-AHTPC scheme is prosed for the developed ankle rehabilitation robot. Instead of conventional assisted-as-needed studies utilizing only position feedback or impedance parameter, the proposed ET-AHTPC achieves the online synchronous torque-position adjustment according to the patient's rehabilitation state and training performance. Based on the Brunnstrom clinical scale, a robot-assisted rehabilitation index is introduced to the proposed adaptive torque controller and the robotic assistance can be adjusted adaptively according to patient's motor ability. A novel critic NN-based event-triggered controller effectively reduces updates of the control law, achieving fast-response and naturally synchronous torque-position adjustment for practical robotic rehabilitation. As the rehabilitation requirement and assessment in clinical practice are more complicated, further studies and clinical trials of the ET-AHTPC will be conducted for ankle rehabilitation.

APPENDIX

A. Derivation of the robot dynamics

According to the assembly relation of the three rotation axes of the robot, the parallel mechanism can be regarded as a 3-DOF serial robot. Its special feature is that the three joint rotation axes of the serial robot intersect at one point. The following parameters marked by 1/2/3 are corresponding to X/Y/Z axis respectively. According to the D-H method, the homogeneous transformation matrix is used to describe the coordinate changes between adjacent DOF.

The element M_{ij} and G_i $(i = 1,2,3; j = 1,2,3)$ in the inertia matrix $M(q)$ and gravity vector $G(q)$ in (1) can be expressed as

$$M_{ij} = \sum_{k=max(i,j)}^{3} Trace(U_{kj} J_k U_{ki}^T)$$
$$G_i = \sum_{k=i}^{3} -m_k g U_{ki} r_{k-1} \quad \text{(A1)}$$

where g is the gravity acceleration, m_i is the mass of the joint of ith-axis, and r_i is the coordinate of the centroid of the joint of ith-axis with the coordinate system of $(i+1)$th-axis. J_i is the pseudo inertia matrix of the ith-axis, and U_{ij} is related to the homogeneous transformation matrix.

The element C_{ij} $(i = 1,2,3; j = 1,2,3)$ in the Coriolis force matrix $C(q, \dot{q})$ in (1) is

$$C_{ij} = \sum_{k=1}^{3} \sum_{k=max(i,j,h)}^{3} Trace\left(\frac{\partial U_{ij}}{\partial q_k} J_k U_{ki}^T\right) \dot{q}_k \quad \text{(A2)}$$

B. Derivation of (15) and (16)

From (13), we have

$$y^T \beta_y y + \Lambda_1 \Lambda_\beta \Lambda_1^T = y^T \beta_y y + \hat{s}^T \alpha_\tau \hat{s}^T + \frac{1}{2} e_\Delta^T \beta_e \hat{s}^T + \frac{1}{2} \hat{s}^T \beta_e e_\Delta^T + e_\Delta^T \beta_1 \beta_e e_\Delta^T \quad \text{(B1)}$$

where α_τ and β_e satisfy the condition $\beta_1 \lambda_{\min}[\alpha_\tau] \geq \frac{1}{4} \lambda_{\max}[\beta_e]$, and $\lambda_{\min}[\cdot]$ and $\lambda_{\max}[\cdot]$ are the corresponding minimum and maximum eigenvalues of the matrices. Λ_β is positive definite, thus $y^T \beta_y y + \Lambda_1 \Lambda_\beta \Lambda_1^T \geq 0$ in (15) is proved. Based on (7), $\hat{s}^T(\varepsilon_{intc} + \tau_{int})$ in (13) could be presented as (B2), and (16) is obtained.

$$\hat{s}^T(\varepsilon_{intc} + \tau_{int}) = \hat{s}^T \left(-\frac{s^T \tau_{int} + \sigma}{\|s^T \tau_{int}\| + \sigma} \tau_{int} + \tau_{int} \right) \quad \text{(B2)}$$

REFERENCES

[1] S. S. Virani, A. Alonso, H. J. Aparicio, E. J. Benjamin, and C. W. Tsao, "Heart Disease and Stroke Statistics—2021 Update: A Report From the American Heart Association," *Circulation,* vol. 141, 2021.

[2] D. Lubbe, E. Lakhani, J. W. Brantingham, G. F. Parkin-Smith, and C. Korporaal, "Manipulative Therapy and Rehabilitation for Recurrent Ankle Sprain With Functional Instability: A Short-Term, Assessor-Blind, Parallel-Group Randomized Trial," *J Manip Physiol Ther,* vol. 38, pp. 22-34, 2015.

[3] C. J. Winstein, J. Stein, R. Arena, B. Bates, L. R. Cherney, *et al.*, "Guidelines for Adult Stroke Rehabilitation and Recovery A Guideline for Healthcare Professionals From the American Heart Association/American Stroke Association," *Stroke,* vol. 47, pp. 98-169, 2016.

[4] M. Wei, Q. X. Sheng, L. Quan, C. Z. Lu, and Q. Ai, "Robust Iterative Feedback Tuning Control of a Compliant Rehabilitation Robot for Repetitive Ankle Training," *IEEE/ASME Trans Mech,* vol. 22, pp. 173-184, 2017.

[5] H. J. Asl, M. Yamashita, T. Narikiyo, and M. Kawanishi, "Field-Based Assist-as-Needed Control Schemes for Rehabilitation Robots," *IEEE/ASME Trans Mech,* vol. 25, pp. 2100-2111, Aug 2020.

[6] O. Baser, H. Kizilhan, and E. Kilic, "Employing variable impedance (stiffness/damping) hybrid actuators on lower limb exoskeleton robots for stable and safe walking trajectory tracking," *J Mech Sci Tech,* vol. 34, pp. 2597-2607, Jun 2020.

[7] M. Escamilla, D. Ortiz, I. Salgado, and I. Chairez, "Hybrid position/force output feedback second-order sliding mode control for a prototype of an active orthosis used in back-assisted mobilization," *Med Biol Eng Comput,* vol. 57, pp. 1843-1860, Sep 2019.

[8] B. Ghannadi, R. S. Razavian, and J. McPhee, "Configuration-Dependent Optimal Impedance Control of an Upper Extremity Stroke Rehabilitation Manipulandum," *Frontiers in Robotics and AI,* vol. 5, Nov 2018.

[9] A. Mancisidor, A. Zubizarreta, I. Cabanes, P. Bengoa, A. Brull, *et al.*, Jung, "Inclusive and seamless control framework for safe robot-mediated therapy for upper limbs rehabilitation," *Mechatronics,* vol. 58, pp. 70-79, Apr 2019.

[10] N. Naghavi, A. Akbarzadeh, S. M. Tahamipour-Z, and I. Kardan, "Assist-As-Needed control of a hip exoskeleton based on a novel strength index," *Robot Auton Syst,* vol. 134, pp. 1-10, Dec 2020.

[11] X. Li, Y. P. Pan, G. Chen, and H. Y. Yu, "Multi-modal control scheme for rehabilitation robotic exoskeletons," *Int J Robot Res,* vol. 36, pp. 759-777, Jun 2017.
[12] Q. S. Ai, D. Ke, J. Zuo, W. Meng, Q. Liu, Z. Q. Zhang, *et al.*, "High-Order Model-Free Adaptive Iterative Learning Control of Pneumatic Artificial Muscle With Enhanced Convergence," *IEEE T Ind Electron,* vol. 67, pp. 9548-9559, Nov 2020.
[13] C. X. Mu and K. Wang, "Approximate-optimal control algorithm for constrained zero-sum differential games through event-triggering mechanism," *Nonlinear Dynam,* vol. 95, pp. 2639-2657, Mar 2019.
[14] R. R. Nair, L. Behera, and S. Kumar, "Event-Triggered Finite-Time Integral Sliding Mode Controller for Consensus-Based Formation of Multirobot Systems With Disturbances," *IEEE T Contr Syst T,* vol. 27, pp. 39-47, Jan 2019.
[15] A. Sinha, R. Kumar, R. Kaur, and R. K. Mishra, "Consensus-Based Odor Source Localization by Multiagent Systems Under Resource Constraints," *IEEE T Cy,* vol. 50, pp. 3254-3263, Jul 2020.
[16] A. Nandanwar, N. K. Dhar, D. Malyshev, L. Rybak, and L. Behera, "Finite-Time Robust Admissible Consensus Control of Multirobot System Under Dynamic Events," *IEEE Syst J,* vol. 15, pp. 780-790, Mar 2021.
[17] A. Lv, C. Pslb, B. Mb, A. Is, D. Cob, and C. Icb, "Event driven sliding mode control of a lower limb exoskeleton based on a continuous neural network electromyographic signal classifier," *Mechatronics,* vol. 72, pp. 1-15, 2020.
[18] J. Wang, J. Liu, G. Zhang, and S. Guo, "Periodic event-triggered sliding mode control for lower limb exoskeleton based on human–robot cooperation," *Isa T,* 2021.
[19] M. Abbas, S. Al Issa, and S. K. Dwivedy, "Event-Triggered Adaptive Hybrid Position-Force Control for Robot-Assisted Ultrasonic Examination System," *J Intell Robot Syst,* vol. 102, pp. 1-19, Aug 2021.
[20] X. W. Wu and C. Q. Wang, "Event-driven adaptive near-optimal tracking control of the robot in aircraft skin inspection," *Int J Robust Nonlin,* vol. 31, pp. 2593-2613, May 2021.
[21] M. Hwang, B. Thananjeyan, S. Paradis, D. Seita, J. Ichnowski, D. Fer, *et al.*, "Efficiently Calibrating Cable-Driven Surgical Robots with RGBD Fiducial Sensing and Recurrent Neural Networks," *IEEE Robot Autom Let,* vol. PP, pp. 1-1, 2020.
[22] C. F. Juang and T. B. Bui, "Reinforcement Neural Fuzzy Surrogate-Assisted Multiobjective Evolutionary Fuzzy Systems With Robot Learning Control Application," *IEEE T Fuzzy Syst,* vol. 28, pp. 434-446, 2020.
[23] Y. J. Choo, J. K. Kim, J. H. Kim, M. C. Chang, and D. Park, "Machine learning analysis to predict the need for ankle foot orthosis in patients with stroke," *Scientific Reports,* vol. 11, pp. 1-7, Apr 2021.
[24] Q. Liu, J. Zuo, C. X. Zhu, W. Meng, Q. S. Ai, and S. Q. Xie, "Design and Hierarchical Force-Position Control of Redundant Pneumatic Muscles-Cable-Driven Ankle Rehabilitation Robot," *IEEE Robot Autom Let,* vol. 7, pp. 502-509, Jan 2022.
[25] T. Li, D. Yang, X. Xie, and H. Zhang, "Event-Triggered Control of Nonlinear Discrete-Time System With Unknown Dynamics Based on HDP(lambda)," *IEEE T Cy,* 2021.
[26] S. Zhang, B. Zhao, D. Liu, and Y. Zhang, "Observer-based event-triggered control for zero-sum games of input constrained multi-player nonlinear systems," *Neural Networks,* vol. 144, pp. 101-112, Dec 2021.
[27] D. Wang, H. He, and D. Liu, "Adaptive Critic Nonlinear Robust Control: A Survey," *IEEE T Cy,* vol. 47, pp. 3429-3451, Oct 2017.
[28] Y. H. Zhu, D. B. Zhao, H. B. He, and J. H. Ji, "Event-Triggered Optimal Control for Partially Unknown Constrained-Input Systems via Adaptive Dynamic Programming," *IEEE T Ind Electron,* vol. 64, pp. 4101-4109, 2017.
[29] D. S. Yang, T. Li, X. P. Xie, and H. G. Zhang, "Event-Triggered Integral Sliding-Mode Control for Nonlinear Constrained-Input Systems With Disturbances via Adaptive Dynamic Programming," *IEEE T Syst Man Cybern Syst,* vol. 50, pp. 4086-4096, Nov 2020.
[30] Shuping, Haiyang, Fang, Maoguang, Zhang, Fei, *et al.*, "Adaptive Optimal Control for a Class of Nonlinear Systems: The Online Policy Iteration Approach," *IEEE T Neural Networ Learn Syst,* 2019.
[31] S. Ding, J. Z. Peng, H. Zhang, and Y. N. Wang, "Neural network-based adaptive hybrid impedance control for electrically driven flexible-joint robotic manipulators with input saturation," *Neurocomputing,* vol. 458, pp. 99-111, Oct 2021.
[32] H. Navvabi and A. H. D. Markazi, "Hybrid position/force control of Stewart Manipulator using Extended Adaptive Fuzzy Sliding Mode Controller (E-AFSMC)," *Isa T,* vol. 88, pp. 280-295, May 2019.
[33] E. Akdogan, M. E. Aktan, A. T. Koru, M. S. Arslan, M. Athhan, and B. Kuran, "Hybrid impedance control of a robot manipulator for wrist and forearm rehabilitation: Performance analysis and clinical results," *Mechatronics,* vol. 49, pp. 77-91, Feb 2018.
[34] C. H. Lin, Y. Y. Su, Y. H. Lai, and C. C. E. Lan, "A Spatial-Motion Assist-as-Needed Controller for the Passive, Active, and Resistive Robot-Aided Rehabilitation of the Wrist," *IEEE Access,* vol. 8, pp. 133951-133960, 2020.
[35] Q. T. Dao and S. I. Yamamoto, "Assist-as-Needed Control of a Robotic Orthosis Actuated by Pneumatic Artificial Muscle for Gait Rehabilitation," *Applied Sciences-Basel,* vol. 8, Apr 2018.

Jie Zuo received the B.S. degree in information engineering from Wuhan University of Technology, Wuhan, China, in 2015. Since 2016, she has been studying as a student with successive postgraduate and doctoral programs at Wuhan University of Technology. Her research interests include rehabilitation robots modelling and motion control.

Quan Liu received the Ph.D. degree in mechanical engineering in 2004 from Wuhan University of Technology, Wuhan, China, where she is currently a Chair Professor in information engineering. She authored more than 80 technical publications, proceedings, editorials, and books. She has directed more than 20 research projects. Her research interests include signal processing, robots and electronics. Dr. Liu received two national awards and three provincial and ministerial awards.

Wei Meng received his Ph.D. degree jointly by Wuhan University of Technology, China and The University of Auckland, New Zealand in 2016. He was a Research Fellow in the School of Electronic and Electrical Engineering, University of Leeds, UK from 2018 to 2020. He is now an Associate Professor at Wuhan University of Technology. His research interests include robot-assisted rehabilitation, human–robot interaction, and control. He has directed 3 national research projects, co-authored 4 books, published over 60 journal and conference papers.

Qingsong Ai received his M.S. and Ph.D. degrees from Wuhan University of Technology, China, in 2006 and 2008, respectively. From 2006 to 2007, he was a visiting researcher at the University of Auckland, New Zealand. He is currently a full Professor at the Wuhan University of Technology and Hubei university. Prof. Ai is the project leader of 12 national, ministerial or provincial projects with the total amount of 13M RMB. He has published over 70 international journal papers. His research interests include signal processing, rehabilitation robots and manufacturing technology.

Sheng Q. Xie (SM'11) received his Ph.D. degrees from Huazhong University of Science and Technology, China and University of Canterbury, New Zealand, in 1998 and 2002, respectively. He joined The University of Auckland in 2003 and became a Chair Professor in (bio)mechatronics in 2011. Since 2017 Prof Xie has been the Chair in Robotics and Autonomous Systems at University of Leeds. He has published 7 books, 15 book chapters, and over 400 international journal and conference papers. His research interests are medical and rehabilitation robots, advanced robot control. Prof. Xie is an elected Fellow of The Institution of Professional Engineers New Zealand (FIPENZ). He has also served as a Technical Editor for IEEE/ASME TRANSACITONS ON MECHARTEONICS.